Journal of Nuclear Materials 468 (2016) 164–170

Contents lists available at ScienceDirect

Journal of Nuclear Materials

journal homepage: www.elsevier.com/locate/jnucmat

Atomic simulations of Fe/Ni multilayer nanocomposites on the radiation damage resistance

Feida Chen [a], Xiaobin Tang [a, b, *], Yahui Yang [a], Hai Huang [a], Jian Liu [a], Huan Li [a], Da Chen [a, b]

[a] Department of Nuclear Science & Engineering, Nanjing University of Aeronautics and Astronautics, Nanjing, China
[b] Jiangsu Key Laboratory of Nuclear Energy Equipment Materials Engineering, Nanjing, China

ARTICLE INFO

Article history:
Received 6 September 2015
Received in revised form
15 November 2015
Accepted 17 November 2015
Available online xxx

Keywords:
Fe/Ni multilayers
Molecular dynamics
Radiation damage resistance
Orientation relationship

ABSTRACT

We investigated the radiation damage resistance of the Fe/Ni multilayer nanocomposites by molecular dynamics. In the paper, two types of interface configuration with different orientation relationship were constructed. Their morphology evolution and number of final surviving defects induced by cascade collisions were discussed respectively. The interfaces of the two types of Fe/Ni multilayers kept distinct during the long-time relaxation before cascade. The comparison of surviving defects number produced by PKA with 5 keV at 100 K showed that the Fe/Ni multilayers have greater radiation tolerance than that of the bulk materials. However, the orientation relationship of the interface influences the defects self-healing capability greatly when the multilayers are irradiated by higher energy PKA or at high temperature. The radiation damage resistance of the Nishiyama – Wassermann type Fe/Ni multilayers which have larger lattice misfit is more stable than that of the Kurdjumov – Sachs type.

1. Introduction

Materials in the extreme irradiation environments induced by the advanced nuclear reactor systems will suffer severe damages such as swelling [1] and embrittlement [2], which are known as consequences of the accumulation of radiation-induced point defects [3,4]. Therefore, improving the intrinsic ability of materials in the form of trapping and absorbing radiation-induced defects is regarded as an effective approach to design ultra high radiation resistance materials [5]. Since it has been proved that the pre-existing dislocation structures [6], grain boundaries [7] and interfaces [8] in materials can act as sinks for defects in previous studies, the increasing attention was paid world-widely to the metallic multilayer nanocomposites which contain abundant interface regions [9–11].

Using the Cu/Nb multilayer nanocomposites as a model system, Demkowicz et al. investigated the cascade collision process and physics mechanisms of interactions between interfaces and radiation-induced defects by molecular dynamics simulation [12,13]. The results showed that the Cu/Nb interfaces can trap large fluxes of vacancies and interstitials, and enhance their recombination, which drives the nanocomposites to evolve from disorder state to a damage-free steady state. In order to expand the range of composing element selection options and open the door to the practical application in nuclear reactor structure materials, further researches on a class of low neutron activation, radiation damage self-healing multilayer nanocomposites will still need to be done. In the present paper, we focused on a kind of low neutron activation, bcc/fcc type metallic multilayer nanocomposites composed of iron and nickel. These two elements are widely used in many nuclear reactor components [14,15]. In the previous study, we prepared the Fe/Ni multilayers by magnetron sputtering and investigated its properties after being exposed to the ions irradiation at different temperature [16]. Although a new $FeNi_3$ phase formed after the irradiation, the interfaces between Fe layers and Ni layers kept distinct. However, it is difficult to discuss the defects self-healing performance of the Fe/Ni multilayers by experimental approach, because the radiation-induced point defects are invisible even in the high-resolution transmission electron microscopy (HRTEM) images. In the present paper, we investigated the defects evolution process in Fe/Ni multilayers induced by cascade collision using molecular dynamics simulation and compared its self-

* Corresponding author. Department of Nuclear Science & Engineering, Nanjing University of Aeronautics and Astronautics, Nanjing, China.
E-mail address: tangxiaobin@nuaa.edu.cn (X. Tang).

http://dx.doi.org/10.1016/j.jnucmat.2015.11.028
0022-3115/

healing performance with the bulk iron and nickel.

Four major types of crystallographic orientation relationships can be formed between the adjacent bcc and fcc nanolayeres: Kurdjumov-Sachs (KS), Nishiyama-Wassermann (NW), Pitsch, and Bain orientation relationships [17]. Here, we discussed effects of the two common interface orientation relationships (KS and NW) [18] on the radiation damage resistance of Fe/Ni multilayer nanocomposites.

2. Interface configuration and MD simulation method

2.1. Atomic structures of Fe/Ni interfaces

Two Fe/Ni multilayer models with the KS and the NW orientation relationship were constructed in the work. For the first interface model referred to as KS, two semi-infinite perfect fcc Ni and bcc Fe crystals were assembled directly according to the KS orientation relationship, i. e. $\{111\}_{Ni} \parallel \{110\}_{Fe}$. Furthermore, the crystallographic direction $[11\bar{2}]_{Ni} \parallel [1\bar{1}2]_{Fe} \parallel$ x-axis and $[\bar{1}10]_{Ni} \parallel [1\bar{1}\bar{1}]_{Fe} \parallel$ y-axis. As shown in Fig. 1(a), the Ni layer has 29 periodicity-lengths along $[11\bar{2}]$, 166.885 Å, and has 25 periodicity-lengths along $[\bar{1}10]$, 124.592 Å; the Fe layer has 35 periodicity-lengths along $[1\bar{1}2]$, 167.839 Å, and has 25 periodicity-lengths along $[1\bar{1}\bar{1}]$, 123.625 Å. The model's dimensions can't be determined arbitrarily because the periodic boundary condition requires equal dimensions in the Fe and Ni layers. The second interface model referred to as NW was created in the same way described above. As shown in Fig. 1(b), the NW interface model was formed by $\{111\}_{Ni} \parallel \{110\}_{Fe}$, while $[211]_{Ni} \parallel [110]_{Fe} \parallel$ x-axis and $[01\bar{1}]_{Ni} \parallel [001]_{Fe} \parallel$ y-axis. The Ni layer has 30 periodicity-lengths along [211], 172.640 Å, and has 35 periodicity-lengths along $[01\bar{1}]$, 174.429 Å; the Fe crystal has 43 periodicity-lengths along [110], 173.616 Å, and has 61 periodicity-lengths along [001], 174.155 Å. The heights of Ni and Fe layers in the z-axis were chosen to be 80 Å each in the two models.

Before relaxation, the atomic structures of the first Fe plane adjacent to the Fe/Ni boundary of the KS and NW interfaces were shown in Fig. 2. The atoms were colored according to their potential energy, in order to show the misfit dislocation distribution in the interface clearly. The patterns formed on the KS and NW interfaces were distinct from each other. For the KS interface, there is only 1 set of dislocation paralleled to the y-axis because the lattice mismatch between the $[\bar{1}10]_{Ni}$ (4.984 Å) and $[1\bar{1}\bar{1}]_{Fe}$ (4.965 Å) is only 0.38%, while the lattice mismatch between the $[11\bar{2}]_{Ni}$ (7.021 Å) and $[1\bar{1}2]_{Fe}$ (8.632 Å) changes periodically with the increasing of x position. For NW interface, the dislocation pattern seemed much more complicated. 3 sets of dislocation can be observed and atoms located on their intersections showed the highest potential energy in the overall interface.

An interfacial region can also be clearly identified according to the average cohesive energies of atoms on each plane adjacent to the interface after relaxation [19]. As illustrated in Fig. 3, the average cohesive energies of the nearest one plane of Fe and Ni are appreciably higher than the bulk region (i.e. region far away from the interface). Existence of the lattice mismatch between the Fe and Ni layers may be the main reason for the peculiar increase. Since there is severe lattice distortion in the interfacial region, atoms in this region wouldn't be taken into account when we calculate the surviving defect numbers induced by cascade collision.

2.2. Simulation method for cascade collision

The periodic boundary conditions were applied in three directions. An embedded atom method (EAM) potential developed by K. Vortler et al. was used for Fe–Ni system [20]. The potential has been modified with ZBL potential and has been verified for cascade collision simulation [14].

The cascade collision simulation model contains two parts: the free region and the fixed region. Region within the distance of 5 Å away from the simulation box boundary was set as fixed region and maintained its temperature at constant by using a Nose-Hoover heat bath, while all atoms in the whole system were fixed in the NVE ensemble. The cascade was then conducted by giving a selected Fe atom a large velocity perpendicularly towards the Fe/Ni interface to simulate the radiation damage process produced by the primary knocked-on atom (PKA). The distance between the selected Fe atoms and the Fe/Ni interface in the z-axis was determined by the calculation results of a Monte Carlo code SRIM [21], which are shown in Fig. 4. The simulation was allowed to evolve for 50 ps with a varying time-step until reaching a steady state with no significant defect evolution.

In our work, effects of (i) orientation relationship of interface, (ii) energy of PKA, and (iii) temperature of system on the radiation damage resistance were argued. Each type of cascade collision was simulated ten times (by the means of selecting different atoms located near the center of x-y plane) and calculated their mean value.

Additionally, cascade collisions were also simulated in the bulk bcc Fe crystals and the bulk fcc Ni crystals for comparison. To

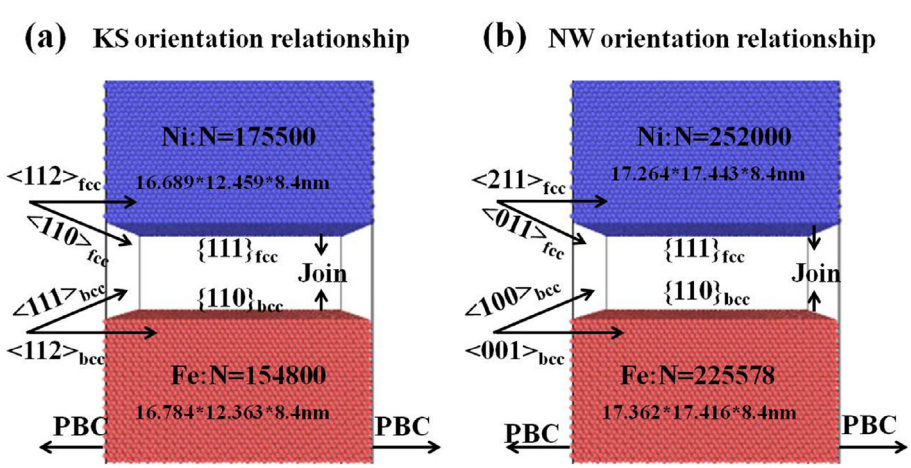

Fig. 1. (a) The Fe/Ni multilayer model with the KS orientation relationship; (b) The Fe/Ni multilayer model with the NW orientation relationship (Fe and Ni atoms are shown as red and blue, respectively). (For interpretation of the references to colour in this figure legend, the reader is referred to the web version of this article.)

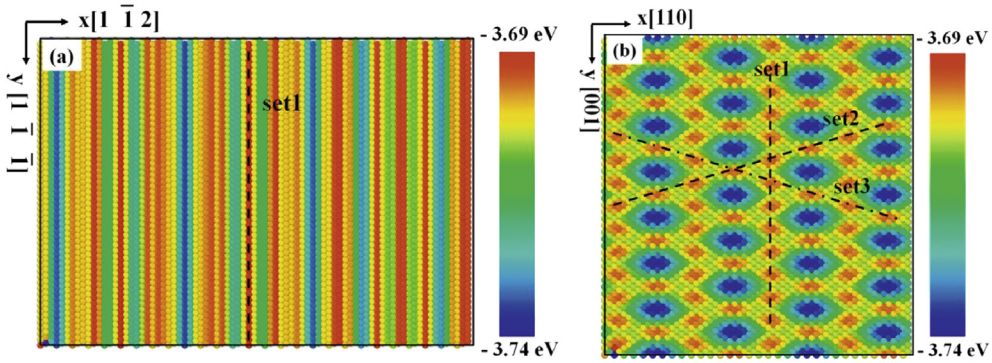

Fig. 2. The interface structure of the first Fe plane adjacent to Fe/Ni boundary (a) KS interface; (b) NW interface (Atoms are colored according to their potential energy).

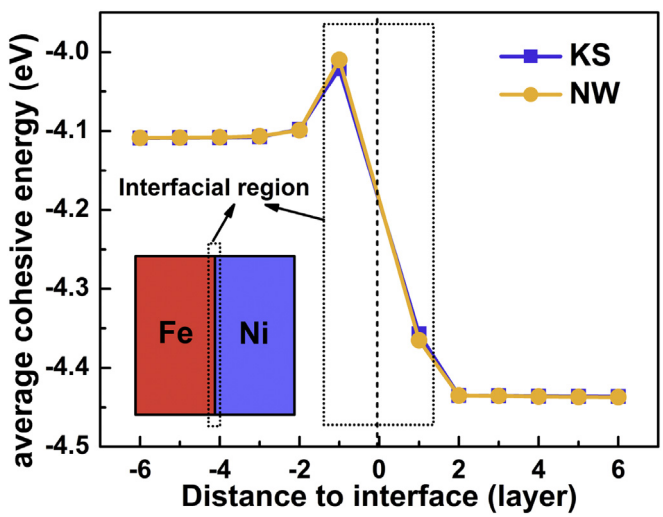

Fig. 3. The average cohesive energies of atoms varying with the distance from the Fe/Ni interface. The positive layer number stands for the nickel layer, while the negative layer number stands for the iron layer.

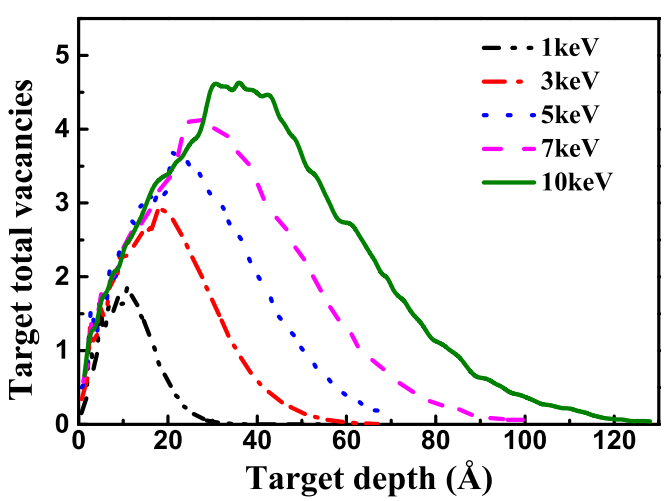

Fig. 4. Damage depth in the Fe/Ni multilayers induced by PKA at 1, 3, 5, 7, and 10 keV. The calculation results of SRIM presented the most damaged depth of different PKA energy cases. According to these curves, the most suitable distance between PKAs and the interface were selected to be 10 Å, 17 Å, 20 Å, 22 Å, and 35 Å for the 1, 3, 5, 7, and 10 keV PKA cases, respectively.

exclude the influence of the incident direction of PKA, the coordinate axis of the bulk bcc Fe and fcc Ni crystals need to be rotated accordingly. The rotated bulk metal models were referred to as "KS Fe", "KS Ni", "NW Fe", and "NW Ni" below for convenience. The detailed coordinate axis information was listed in Table 1. In all simulations, the incident direction of PKAs was kept along z-axis.

All simulations were carried out with LAMMPS code [22] and visualized with OVITO [23].

3. Results and discussion

3.1. Thermal stability of Fe/Ni multilayers

Relaxation simulations at elevated temperature were performed before the cascade collision simulation to investigate the interface stability for the hypothesized Fe/Ni system. After relaxation at a constant temperature for 1 ns, the cross section view and radial distribution function of Fe/Ni multilayer are shown in Fig. 5. In order to show the intermixing between Fe and Ni slabs, we presented two cross section view of the same relaxation KS interface model at 1700 K in Fig. 5(a) and (b). In Fig. 5(a), only Ni atoms are shown, while Fig. 5(b) only shows Fe atoms. A distinct interface appears between the Fe and Ni crystal slabs, which demonstrates that there is little intermixing even at 1700 K. However, when the temperature was raised to 1900 K (exceeds the melting point), Fe and Ni atoms adjacent to the interface diffuse into each other apparently, as shown in Fig. 5(c) and (d). On the other hand, the radial distribution function of Fe crystal slab (Fig. 5(e)) and Ni crystal slab (Fig. 5(f)) turns wider as temperature rises up. These figures show that though the crystalline structure of metals tends to be out of order as the temperature rises up, the Fe/Ni interface is stable during the time scale of simulation. The same feature can be observed in the NW interface.

3.2. Radiation damage resistance under cascade collision

In this section the cascade collision was started by a PKA with 5 keV. During the whole simulation, the system temperature was maintained 100 K. Since our interest in this study, however, is to

Table 1
Coordinate axis information of the rotated bulk metal models used in the cascade collision simulation.

	x-axis	y-axis	z-axis	PKA incident direction
KS Fe	[1$\bar{1}$ 2]	[1$\bar{1}\bar{1}$]	[110]	[110]
KS Ni	[11$\bar{2}$]	[$\bar{1}$ 10]	[111]	[111]
NW Fe	[110]	[001]	[1$\bar{1}$ 0]	[1$\bar{1}$ 0]
NW Ni	[211]	[01$\bar{1}$]	[$\bar{1}$ 11]	[$\bar{1}$ 11]

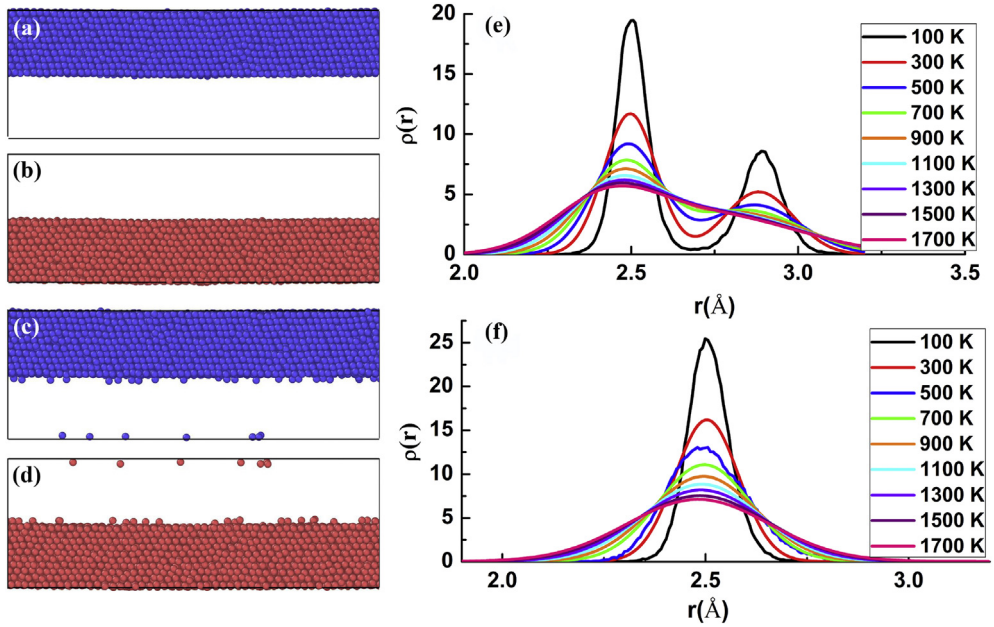

Fig. 5. Cross section view and radial distribution function of Fe/Ni multilayer after relaxation: (a) and (b) show the cross section view of the KS interface at 1700 K. The Fe atoms in (a) and Ni atoms in (b) were deleted; (c) and (d) show the cross section view of the KS interface at 1900 K. The Fe atoms in (c) and Ni atoms in (d) were deleted; (e) radial distribution function of Fe crystal slab; (f) radial distribution function of Ni crystal slab.

argue the influence of Fe/Ni interface on the radiation damage resistance performance, the energy of PKA and system temperature were chosen arbitrarily and their effects will be discussed in the next section. Number of vacancies and interstitials produced in the cascade collision outside the interfacial region, which has been described in Sec. 2.1, was identified as conventional point defects using the Wigner-Seitz defect analysis method [24]. Note that unlike in bulk Fe and Ni, the number of vacancies and interstitials need not be equal because in each simulation a different number of these defects may have been trapped in the interfacial region [25].

Fig. 6(a) and (b) show the evolution of number of point defects (vacancies (shown in 6(a)) and interstitials (shown in 6(b)), respectively) in the Fe/Ni KS interface model and the NW interface model in one cascade collision simulation, compared with cases in the bulk bcc Fe and fcc Ni. In the two figures, the cascade peak reaches maximum value in 0.5 ps for all cases and has stable defects after about 4 ps of the simulation time.

In Fig. 6(c), we compared the surviving defects number for all the cases. It is clear that both the vacancies and interstitials in the multilayer model are much fewer than those in the bulk bcc Fe and fcc Ni during the whole process. It indicates that, when irradiated by 5 keV PKA at 100 K, the Fe/Ni multilayers have greater radiation tolerance than the bulk materials. The effects of PKA energies and system temperature on radiation damage resistance performance will be discussed further in the next section.

3.3. Effects of elevated PKA energies and system temperature

Fig. 7 shows the total surviving defects number in different materials (bulk Fe, Ni and Fe/Ni multilayers) and the percentage of defects number in multilayer relative to the corresponding bulk metals at 100 K as the function of PKA energies. The percentage of defects number is calculated using the formula below:

$$A\ (\%) = \frac{2N_{d\_interface}}{N_{d\_Fe} + N_{d\_Ni}}, \tag{1}$$

where $N_{d\_interface}$ is the total surviving defects number of KS or NW Fe/Ni multilayer model; N_{d_Fe} and N_{d_Ni} means the defects number of the corresponding bulk Fe and Ni.

From Fig. 7(a) and (b), it is clear that the total surviving defects number of all the cases increases with the increasing of PKA energies. In order to show the influence of PKA energy on the defects suppression effects of the Fe/Ni multilayers, the percentage of defects number in the Fe/Ni multilayer relative to the corresponding bulk metals is shown in Fig. 7 (c).

According to Fig. 7 (c), with the increasing of PKA energy, the trends of percentage of defects number of the KS Fe/Ni multilayer and the NW Fe/Ni multilayer are significantly different. For the KS Fe/Ni multilayer, the percentage keeps below 60% until the PKA energy reaches 5 keV. After that, the percentage rises up from 30.6% to 70.5% when the PKA energy increases from 5 keV to 10 keV. In contrast to that, the percentage of the NW Fe/Ni multilayer remains about 55% in the five cases we simulated. No significant increase trend can be observed with the increasing PKA energy in the NW Fe/Ni multilayer.

Furthermore, more cascade collision simulations induced by PKAs with 5 keV were performed at 900 K (much closer to the actual temperature in the working condition of materials) to investigate the radiation damage resistance of Fe/Ni interface. As shown in Fig. 8, the high temperature weakens the defects self-healing capacity of the KS type Fe/Ni multilayers seriously, but brings little effects on that of the NW type Fe/Ni multilayers.

From the different influence of high PKA energy and high temperature on the surviving defects number in the two types of Fe/Ni multilayers, it seems that the radiation damage resistance of the NW type Fe/Ni multilayers is more stable than that of the KS type multilayers. However, the detail process and mechanism of the defects evolution may be quite different between the cases of high PKA energy and high temperature.

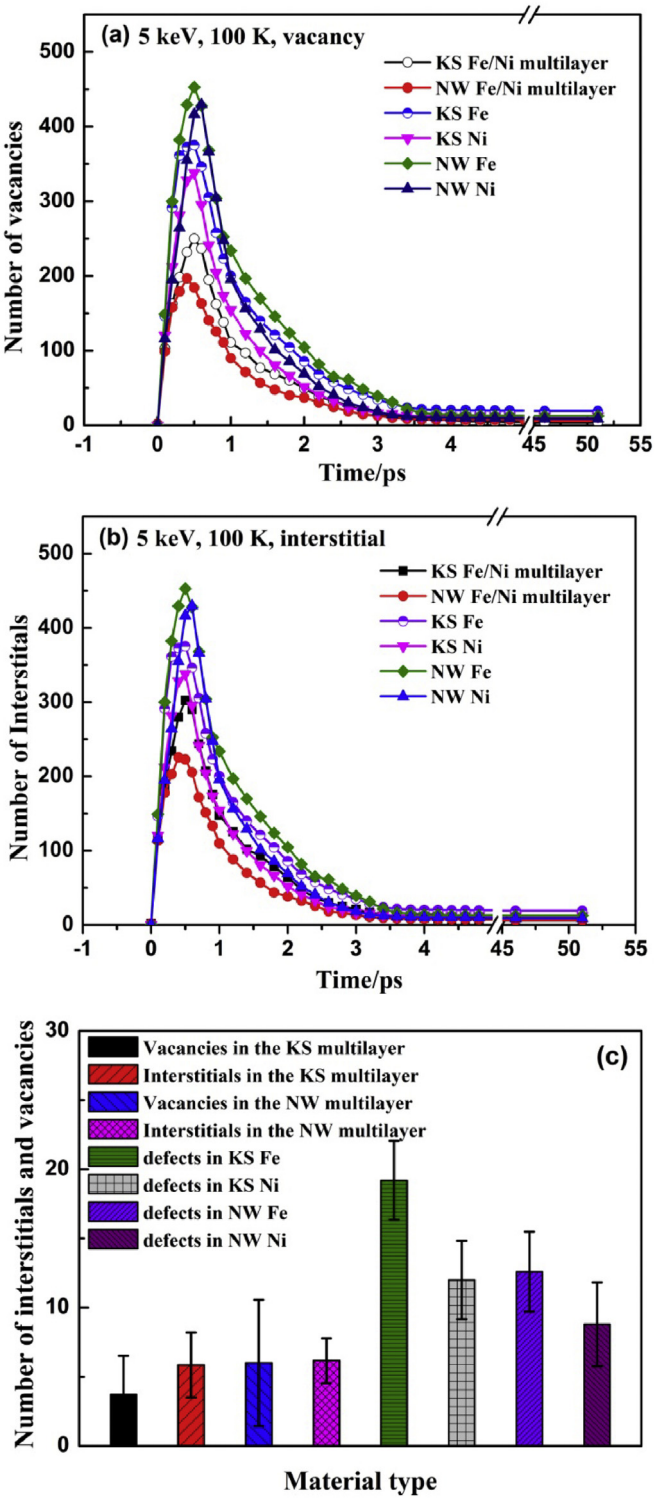

Fig. 6. Number of vacancies and interstitials evolved in the KS and the NW orientation relationship interface models when irradiated by 5 keV PKA at 100 K. (a) and (b) show the number of defects in progress; (c) shows the number of final surviving defects (NW Fe, NW Ni, KS Fe, and KS Ni represent number of defects in bulk iron or nickel whose lattice direction is listed in Table 1; KS interstitials, KS vacancies, NW interstitials, and NW vacancies represent the number of defects in the KS and NW orientation relationship Fe/Ni multilayer models, respectively).

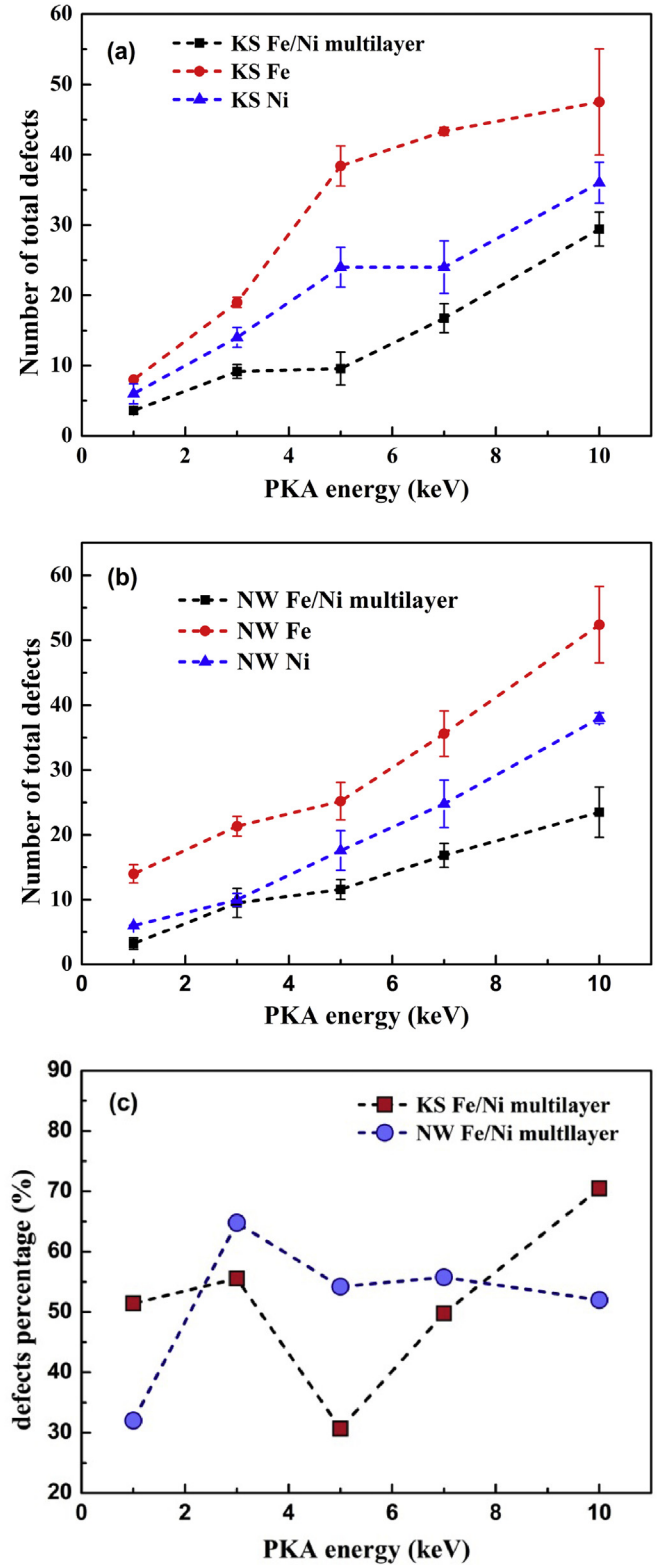

Fig. 7. (a)–(b) The total surviving defects number in different materials (bulk Fe, Ni and Fe/Ni multilayers) when generated by PKA with 1, 3, 5, 7, and 10 keV at 100 K; (c) comparison of the percentage of defects number in the KS and the NW interface multilayers relative to the corresponding bulk metals.

For the case of high PKA energy, the spatial distribution of the displacement cascades core is much larger than that of the low PKA energy case. Although the distances between the PKA and Fe/Ni interface in the simulation are specially selected to ensure that the

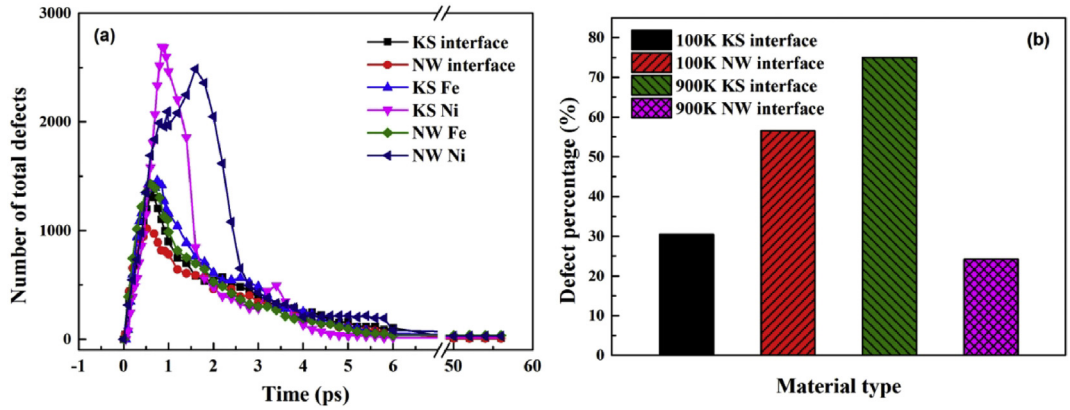

Fig. 8. (a) Evolution of the total point defects number induced by PKAs with 5 keV at 900 K in the KS, NW interface Fe/Ni multilayers and the corresponding bulk metals; (b) comparison of the percentage of defects number in the KS and NW interface multilayers relative to the corresponding bulk metals at 100 K and 900 K.

interface kept in the zone of the cascades core, the cascade front goes farther into the bulk region of the Fe/Ni multilayers and leaves the interface far behind with the increasing of PKA energy. As the interface recedes from these radiation induced defects, its influence on the defects absorption begins to wane. Fig. 9 shows the displacement cascades core in the KS type and NW type Fe/Ni multilayers induced by 5 keV and 10 keV PKA, respectively. Because of the difference of directions of PKA, the increase of cascade core size in the NW model is less than that in the KS model. Hence, the decrease of radiation resistance of the NW type Fe/Ni multilayers is slight in comparison with that of the KS type Fe/Ni multilayers. It is not only the interface configuration, but also the distance between the defects and interface that plays an important role in the issue when system suffers high energy PKA bombardment.

In contrast, the influence of high temperature on the surviving defects number may be mainly determined by the interface configuration. As described in Sec. 2.1, the lattice misfit between the Fe and Ni layers of the KS type model is rather small. In the high temperature system, atoms become mobile and severe lattice distortion takes place in the Fe and Ni layers. This phenomenon makes the small misfit of the Fe/Ni interface decreases further, which weakens the defects trapping capabilities of the KS type Fe/Ni multilayers appreciably. For the NW type Fe/Ni multilayers, however, the lattice misfit is large enough to eliminate the influence of temperature on the lattice distortion. Thus, the surviving defects number of the high temperature case is observed even less than that of the low temperature case. From this point of view, the NW type Fe/Ni multilayers have more stable radiation damage resistance than that of the KS type Fe/Ni multilayers when irradiated at higher temperature condition.

4. Conclusion

We have focused on the radiation damage resistance of a bcc/fcc

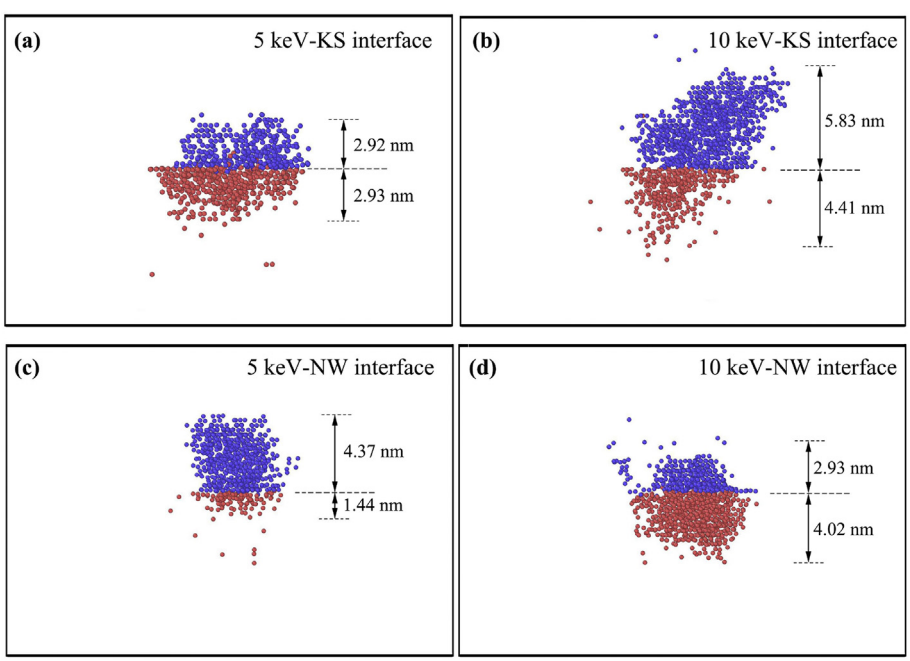

Fig. 9. Spatial distribution of the displacement cascades core in the KS type and NW type Fe/Ni multilayers induced by 5 keV and 10 keV PKA: (a) cascade core in the KS type interface model induced by 5 keV PKA; (b) cascade core in the KS type interface model induced by 10 keV PKA; (c) cascade core in the NW type interface model induced by 5 keV PKA; (d) cascade core in the NW type interface model induced by 10 keV PKA.

type multilayer nanocomposite which composed of Fe and Ni. In the paper, two types of interface configuration with different orientation relationship (referred to as KS and NW) were constructed and their morphology evolution under elevated temperature was investigated. The results demonstrated that the two types of interfaces can keep distinct even at 1700 K and the diffusion between Fe slab and Ni slab is not strong. Then, we performed the cascade collision simulation by 5 keV PKA at 100 K on the Fe/Ni multilayer and its corresponding bulk materials. The comparison of number of final surviving defects indicated that the Fe/Ni multilayers have greater radiation tolerance than the bulk materials. More simulation results from cases of different PKA energies and higher system temperature verified this conclusion furthermore. The simulation results at high temperature suggested that the NW type Fe/Ni multilayers have more stable radiation damage resistance than that of the KS type Fe/Ni multilayers.

Acknowledgments

This work was funded by the Priority Academic Program Development of Jiangsu Higher Education Institutions, the Specialized Research Fund for the Doctoral Program of Higher Education of China (SRFDP) (Grant No. 20133218110023), China Postdoctoral Science Foundation (Grant No. 2014M561642), the Jiangsu Planned Projects for Postdoctoral Research Funds (Grant No. 1401091C), the Fundamental Research Funds for the Central Universities, and the Funding of Jiangsu Innovation Program for Graduate Education and the Fundamental Research Funds for the Central Universities (CXZZ13_0159).

References

[1] S. Zinkle, G. Was, Acta Mater. 61 (2013) 735–758.
[2] O. Chopra, A. Rao, J. Nucl. Mater. 412 (2011) 195–208.
[3] D. Bacon, F. Gao, Y. Osetsky, J. Nucl. Mater. 276 (2000) 1–12.
[4] E. Zarkadoula, J. Phys. Condens. Matter 26 (2014) 085401.
[5] X. Bai, A. Voter, R. Hoagland, M. Nastasi, B. Uberuaga, Science 327 (2010) 1631.
[6] T. Allen, G. Was, Radiat. Eff. Solids. 235 (2007) 123–151.
[7] T. Shen, Appl. Phys. Lett. 90 (2007) 263115.
[8] G. Ackland, Science 327 (2010) 1587.
[9] Q. Wei, N. Li, N. Mara, M. Nastasi, A. Misra, Acta Mater. 59 (2011) 6331–6340.
[10] Y. Gao, J. Nucl. Mater. 413 (2011) 11–15.
[11] K. Wei, Chin. Phys. C 32 (2008) 262–264.
[12] M. Demkowicz, R. Hoagland, J. Hirth, Phys. Rev. Lett. 100 (2008) 136102.
[13] M. Demkowicz, P. Bellow, B. Wirth, Mater. Res. Bull. 35 (2010) 992–998.
[14] C. Wang, Nucl. Instrum. Methods B 321 (2014) 49–53.
[15] N. Lazarev, A. Bakai, J. Supercrit, Fluid. 82 (2013) 22–26.
[16] F. Chen, X. Tang, Y. Yang, H. Huang, J. Nucl. Mater. 452 (2014) 31–36.
[17] H. Zhang, F. Ren, M. Hong, J. Mater. Sci. Technol. 30 (2014) 1012–1019.
[18] Y. Gotoh, S. Entani, H. Kawanowa, Surf. Sci. 507–510 (2002) 401–405.
[19] X. Liu, B. Uberuaga, M. Demkowicz, T. Germann, A. Misra, M. Nastasi, Phys. Rev. B 85 (2012) 012103.
[20] K. Vortler, N. Juslin, G. Bonny, J. Phys. Condens. Matter 23 (2011) 355007.
[21] J. Ziegler, M. Ziegler, J. Biersack, Nucl. Instrum. Methods B 268 (2010) 1818–1823.
[22] S. Plimpton, J. Comp. Phys. 117 (1995) 1–19. http://lammps.sandia.gov/.
[23] A. Stukowski, Modell. Simul. Mater. Sci. Eng. 18 (2009) 015012.
[24] N. Park, Y. Kim, H. Seok, S. Han, Nucl. Instrum. Methods B 265 (2007) 547–552.
[25] M. Demkowicz, R. Hoagland, Inter. J. Appl. Mech. 1 (2009) 421–442.